The Astrophysical Journal, 854:41 (13pp), 2018 February 10 https://doi.org/10.3847/1538-4357/aaa7f4

Hidden Universality in the Merger Rate Distribution in the Primordial Black Hole Scenario

Bence Kocsis[1], Teruaki Suyama[2], Takahiro Tanaka[3,4], and Shuichiro Yokoyama[5,6]
[1] Institute of Physics, Eötvös University, Pázmány P. s. 1/A, Budapest, 1117, Hungary
[2] Research Center for the Early Universe (RESCEU), Graduate School of Science, The University of Tokyo, Tokyo 113-0033, Japan
[3] Department of Physics, Kyoto University, Kyoto 606-8502, Japan
[4] Center for Gravitational Physics, Yukawa Institute for Theoretical Physics, Kyoto University, Kyoto 606-8502, Japan
[5] Department of Physics, Rikkyo University, Tokyo 171-8501, Japan
[6] Kavli IPMU (WPI), UTIAS, The University of Tokyo, Kashiwa, Chiba 277-8583, Japan
Received 2017 October 5; revised 2018 January 4; accepted 2018 January 13; published 2018 February 9

Abstract

It has been proposed that primordial black holes (PBHs) form binaries in the radiation dominated era. Once formed, some fraction of them may merge within the age of the universe by gravitational radiation reaction. We investigate the merger rate of the PBH binaries when the PBHs have a distribution of masses around $\mathcal{O}(10)M_\odot$, which is a generalization of the previous studies where the PBHs are assumed to have the same mass. After deriving a formula for the merger time probability distribution in the PBH mass plane, we evaluate it under two different approximations. We identify a quantity constructed from the mass distribution of the merger rate density per unit cosmic time and comoving volume $\mathcal{R}(m_1, m_2)$, $\alpha = -(m_1 + m_2)^2\partial^2 \ln \mathcal{R}/\partial m_1 \partial m_2$, which universally satisfies $0.97 \lesssim \alpha \lesssim 1.05$ for all binary masses independently of the PBH mass function. This result suggests that the measurement of this quantity is useful for testing the PBH scenario.

Key words: black hole physics – gravitational waves – stars: kinematics and dynamics

1. Introduction

Recent detections of gravitational wave events (GW150914, LVT151012, GW151226, GW170104, GW170608, and GW170814) by the LIGO-Virgo collaboration (Abbott et al. 2016b, 2016c, 2017a, 2017b, 2017c) revealed the existence of binary black holes (BHs) in the mass range 8–35 $M_\odot$. These observations clearly demonstrate that there are numerous BH–BH binaries in the universe that have previously eluded the scrutiny of astronomers. The origin of such heavy BHs and the formation of close binary BHs which merge within the age of the universe are widely debated. Various astrophysical scenarios for the explanations of the gravitational wave events are summarized, for instance, in Abbott et al. (2016a) and Miller (2016).

Although only five robustly identified BH–BH binary mergers with GW detections have been reported so far, merger rates are constrained to within 12–240 $\mathrm{Gpc}^{-3}\,\mathrm{yr}^{-1}$ (Abbott et al. 2017a). With the further improvement of GW detectors, we will soon enter the era of *black hole rush*, where a large number of BH–BH binaries are detected with their masses, spins, and locations determined. Those data will serve us important clues to clarify the origin of binary BHs as well as the formation mechanism of the binaries. Clearly, investigations of how various astrophysical scenario producing merging BH binaries can be distinguished by observations will become a fundamentally important topic.

Recently, a collaboration including three of the authors, Sasaki et al. (2016), pointed out that the GW event GW150914 could be merger events of two primordial black holes (PBHs) based on earlier studies (Nakamura et al. 1997; Ioka et al. 1998). In Nakamura et al. (1997) and Ioka et al. (1998), the formation mechanism of the PBH binaries was proposed, and a connection between the PBH binaries and the gravitational wave events from the merger of binary PBHs was given.[7] PBHs stand for BHs that formed in the very early universe much before the epoch of the matter-radiation equality (Carr & Hawking 1974). For instance, in the well-studied scenario, PBHs form from rare high peaks of the primordial density inhomogeneities whose amplitudes are much larger than the standard deviation. In this case, the PBH mass is given by the total energy contained in the Hubble horizon at the formation time,

$$m_{\rm BH} = \gamma \frac{4\pi}{3}\rho H^{-3} \approx 30\,M_\odot \left(\frac{\gamma}{0.2}\right)\left(\frac{T}{30\ \mathrm{MeV}}\right)^{-2}, \qquad (1)$$

where T is the temperature of radiation and $\gamma = \mathcal{O}(1)$ depends on the details of the BH formation. Analytic estimates give $\gamma = 3^{-3/2} \approx 0.2$ (Carr 1975). Other mechanisms of the PBH production are summarized by Carr (2005). After having formed in the very early universe, PBHs stay on the expansion flow of the universe. Even when PBHs are randomly distributed in space without being clustered, there is a small but non-vanishing probability that two neighboring PBHs happen to be much closer than the mean distance. Such PBHs, being initially on the cosmic expansion flow, eventually start to come closer, influenced by their mutual gravity when the cosmic expansion rate becomes too low to separate them apart. As was shown by Nakamura et al. (1997), a direct collision is avoided by the tidal effect of other PBHs in their vicinity, which leads to the formation of a PBH binary with a large

[7] There are other papers in which the potential detection of PBHs by LIGO was claimed (Bird et al. 2016; Kashlinsky 2016; Clesse & García-Bellido 2017a). The binary formation path is different from that in Sasaki et al. (2016).

eccentricity. Further, Ali-Haimoud et al. (2017) have recently shown that the tidal field of halos and interactions with other PBHs, as well as dynamical friction by unbound dark matter particles, do not affect PBH binaries significantly. Highly eccentric PBH binaries radiate GWs efficiently, and a fraction of them can merge within 14 billion years.

In Sasaki et al. (2016), under the approximation that all PBHs have the same mass of $30\,M_{\odot}$, it was shown that the expected event rate of the PBH binary mergers is consistent with the one determined by the LIGO-Virgo collaboration after the announcement of GW150914 (Abbott et al. 2016d), if the fraction of cold dark matter in PBHs is about 10^{-3}. This fraction is consistent with existing observational upper limits (Brandt 2016; Horowitz 2016; Carr et al. 2017; Gaggero et al. 2017; Green 2017; Inoue & Kusenko 2017; Koushiappas & Loeb 2017a; Matsumoto et al. 2017; Poulin et al. 2017). So far, the PBH scenario proposed by Sasaki et al. (2016) is successful in explaining the LIGO event GW150914.

In the next decades, many more BH binaries will be detected, which will deliver fruitful statistical information on the merger rates in the two-dimensional BH mass plane (m_1, m_2; see Abbott et al. 2016b; O'Leary et al. 2016; Fishbach & Holz 2017; Gondán et al. 2017b; Kovetz et al. 2017; Mandel et al. 2017; Zevin et al. 2017). The purpose of the present paper is to examine if the mass distribution can be used observationally to test the PBH scenario. The currently announced five robust merger events show some scatter in the BH mass as $(m_1, m_2) = (36^{+5}_{-4}, 29^{+4}_{-4})$ for GW150914, $(14.2^{+8.3}_{-3.7}, 7.5^{+2.3}_{-2.3})$ for GW151226, $(31.2^{+8.4}_{-6.0}, 19.4^{+5.3}_{-5.9})$ for GW170104, $(12^{+7}_{-2}, 7^{+2}_{-2})$ for GW170608, and $(30.5^{+5.7}_{-3.0}, 25.3^{+2.8}_{-4.2})$ for GW170814 in units of solar mass (90% credible intervals; Abbott et al. 2016b, 2016c, 2017a, 2017b, 2017c). In this paper, we estimate the merger rate density in the m_1–m_2 plane predicted by the PBH scenario. We extend the formalism of previous studies (Nakamura et al. 1997; Ioka et al. 1998; Sasaki et al. 2016) to compute the merger event rate to the case in which the PBH mass function is not restricted to a single mass but extends over a mass range between $m_{\rm min}$ and $m_{\rm max}$ with $m_{\rm max}/m_{\rm min} \lesssim 10$.[8] We assume that the PBH mass function does not extend over many orders of magnitude, since in that case the dynamics may not be accurately captured by the simple physical processes adopted by Nakamura et al. (1997), Ioka et al. (1998), and Sasaki et al. (2016). Quite interestingly, we find that the merger rate distribution in this case depends on the mass of the BH binary in a specific way and that a quantity constructed from the mass distribution of the merger rate density per unit time and volume $\mathcal{R}(m_1, m_2)$,

$$\alpha = -(m_1 + m_2)^2 \partial^2 \ln \mathcal{R} / \partial m_1 \partial m_2, \tag{2}$$

is insensitive to the PBH mass function. This distinct feature is advantageous since there is no theoretically tight constraint on the shape of the PBH mass function. Identifying the information in the merger rate density that is insensitive to the BH mass function may be used to discriminate different formation channels (O'Leary et al. 2016; Gondán et al. 2017b; Kovetz et al. 2017; Zevin et al. 2017). This information may be used to obtain the probability of mergers for given BH masses, $P_{\rm intr}(m_1, m_2;$ defined by Equation (25)), which is essential in measuring the underlying BH mass function $f(m)$ itself.

Before closing this section, in Table 1 we list definitions of important symbols that are used in this paper.

The paper is organized as follows. We first develop a formalism to compute the event rate in the PBH scenario which can be applied to the case of a non-monochromatic[9] mass function. Then, we apply the derived formula to evaluate the mass dependence of the merger rate in the (m_1, m_2) BH mass plane and show that the special quantity constructed out of the event rate density becomes almost independent of the PBH mass function.

2. Formation of Binary PBHs

In this section, we derive a formula of the merger rate density as a function of the masses of two BHs comprising the binary.

2.1. Formation and Mass Function of PBHs

There are several mechanisms to form PBHs (Carr 2005). Among them, the most natural and widely investigated mechanism is the direct gravitational collapse of the primordial density perturbation in the radiation dominated universe. In this scenario, when an overdense region containing an extremely high density peak in which the perturbation amplitude is greater than $\delta_{\rm th} = \mathcal{O}(1)$ reenters the Hubble horizon, that region directly collapses to a BH (for the estimation of $\delta_{\rm th}$, see Carr 1975; Harada et al. 2013). Crudely speaking, all the energy inside the Hubble horizon at the time of BH formation turns into the BH. This picture allows us to relate the BH mass to the comoving wavenumber k of the primordial density perturbation as

$$m_{\rm PBH} \sim 20\,M_{\odot} \left(\frac{k}{1\ {\rm pc}^{-1}}\right)^{-2}. \tag{3}$$

There are no direct observational constraints on the probability distribution of density perturbations on such small scales.

Although Equation (3) gives us a simple and approximate estimate of the PBH mass in terms of k, the relation (3) is not precisely correct, since the PBH mass also depends on the amplitude of the density perturbation. Deviation of the actual PBH mass from the horizon mass becomes significant as the amplitude of the density perturbation approaches $\delta_{\rm th}$ (Choptuik 1993; Niemeyer & Jedamzik 1998). Thus, even if the spectrum of the primordial density perturbation is monochromatic, the resulting PBH mass function is not monochromatic (Yokoyama 1998). Furthermore, the power spectrum of the primordial density perturbations needs not be monochromatic. In the paradigm of the standard inflationary cosmology, the primordial density perturbations are produced in the inflationary era preceding the radiation dominated era. Several inflationary models have been proposed to date, with different predictions for the power spectral shape of the primordial density perturbation which lead to different PBH numbers and mass functions (see Carr et al. 2016 and references therein). To a varying degree, these models predict a non-monochromatic power spectrum. Thus, the PBH mass function is generally not concentrated on a single mass.

[8] Recently, such an extension has also been done in Raidal et al. (2017). Our study differs from Raidal et al. (2017) in that our primary purpose is to investigate the universal feature of the merger rate distribution that is insensitive to the PBH mass function.

[9] By "monochromatic mass function," we refer to a population in which all PBHs have the same mass.

Table 1
Definitions of Important Symbols that Are Used in this Paper

Symbols	Meaning
$m_1,\ m_2$	Mass of the individual PBHs in binary
m_t	Total mass m_1+m_2
n_{BH}	Comoving PBH number density
f_{PBH}	Fraction of PBHs in dark matter
$f(m)$	PBH mass function with normalization condition (4)
$\mathcal{R}(m_1, m_2, t)$	Merger rate density per unit cosmic time t and comoving volume
$P_{intr}(m_1, m_2, t)$	Intrinsic merger rate density defined by Equation (25)
α	Universal rate exponent defined by Equation (2)
D	Physical distance between PBHs that form a binary
M_i	Mass of ith outer PBH
D_i	Physical distance to ith outer PBH (see Figure 1)
y_i	Comoving distance to ith outer PBH
θ_i	Angle (see Figure 1)
$\boldsymbol{e}_i$	Vector (see Figure 1 and Equation (15))
x	Comoving distance between PBHs that form a binary
x_{max}	Maximum value of x to form binary (see Equation (9))
z_{dec}	Redshift when PBHs form a binary
t_{dec}	Cosmic time corresponding to z_{dec}
A	Defined by Equation (11)
a	Initial semi-major axis of PBH binary
a_{max}	$a_{max} = x_{max}/(1+z_{eq})$
e	Initial eccentricity of PBH binary
e_m	Maximum eccentricity given by Equation (30)
ζ	Length of $\boldsymbol{\zeta}$ defined by Equation (17)
$F(x, \zeta)$	Probability density of (x, ζ) (see Equation (26))
t	Cosmic time when PBH binary merges
τ	Time delay between binary formation and merger: $\tau = t\text{-}t_{dec}$
β	$\sin(2\theta_1)$ (see Equation (36) and below it)
K	Dimensionless quantity defined by Equation (41)
m_c	Defined by Equation (44)
$G(x)$	Defined by Equation (45)
m_{min}	Minimum PBH mass of flat mass function (47)
m_{max}	Maximum PBH mass of flat mass function (47)
$\tilde{\zeta}$	Defined by $\tilde{\zeta} = (m_t/m_{max})\zeta$ (see section 3.2)
$\sigma, \tilde{\sigma}$	σ defined by Equation (52) and $\tilde{\sigma} = (m_t/m_{max})\sigma$
ξ	Fitting parameter appearing in Equation (53)
ν	Dimensionless quantity defined by Equation (56)
w_m	Defined by Equation (57)

The PBH mass function is determined once the inflation model is fixed and the power spectrum of the primordial density perturbation is computed.[10] Since there is no fiducial inflation model producing PBHs and different models predict different PBH mass functions, we do not restrict our analysis to any particular PBH mass function. As mentioned earlier, our only requirement is that it is confined to the mass range $m_{max}/m_{min} \lesssim 10$. The case where the PBH mass function is extended over many orders of magnitude requires a separate analysis, which is beyond the scope of this paper.

In addition to the mass function, the spatial distribution of PBHs also affects the probability of binary formation. In this study, for simplicity we assume that the distribution of PBHs at their birth is statistically uniform and random in space. However, we also have to keep in mind that primordial clustering of PBHs is also possible and could be an important factor to enhance the merger event rate for a fixed mass fraction of PBHs. We define the PBH mass function $f(m)$ such that $f(m)dm$ is the probability that a randomly chosen PBH has mass in $(m, m+dm)$. Thus, $f(m)$ is normalized as

$$\int_{m_{min}}^{m_{max}} f(m)dm = 1. \quad (4)$$

We denote the comoving PBH number density as n_{BH}. The mean comoving separation between two neighboring BHs is thus given by $n_{BH}^{-1/3}$.

Before closing this subsection, it is important to mention that we do not consider the mass growth of the PBHs following their initial formation. The mass change due to accretion is negligible when PBH is in environments similar to the cosmic average density (Carr & Hawking 1974; Custodio & Horvath 1998; Ali-Haimoud & Kamionkowski 2017). This may not be true for PBHs residing in high density regions of galaxies such as molecular clouds, accretion disks, or stellar interiors. However, since the majority of PBHs are expected to remain mostly in low density regions such as dark matter halos, we ignore the mass growth of PBHs.

[10] In addition, non-Gaussianity of the primordial density perturbation also affects the PBH mass function (Byrnes et al. 2012; Young & Byrnes 2013).

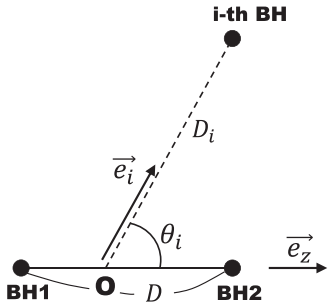

Figure 1. Schematic picture showing the spatial configuration of BHs.

2.2. Semi-major Axis and Eccentricity of a Binary

Just after PBHs are formed in the early universe, they are typically separated by super-Hubble distances. Apart from a possible peculiar velocity, each PBH is attached to the flow of the cosmic expansion. Let us denote the mass of a randomly selected PBH by m_1, and the mass of and the comoving distance to the closest PBH by m_2 and x, respectively. Denoting the physical distance between the two BHs by D (see Figure 1), the gravitational force is given by Gm_1m_2/D^2. Ignoring for the moment the subdominant effects of the other remote BHs and the initial peculiar velocity, and assuming that the above gravitational force is the only dynamical effect acting on each BH,[11] the BHs attract each other and collide within the free-fall time given by

$$t_{\rm ff} = D^{3/2}/\sqrt{Gm_{\rm t}}, \quad m_{\rm t} \equiv m_1 + m_2. \tag{5}$$

In reality, the space is expanding, and the BHs will be distanced if the space expands by $\mathcal{O}(1)$ or more within the free-fall time. Conversely, if the free-fall time is shorter than the Hubble time $1/H$, then the two BHs become gravitationally bound and eventually collide. Since the free-fall time and the Hubble time respectively scale as (scale factor)$^{3/2}$ and (scale factor)^2 during the radiation dominated era, the Hubble time may eventually exceed the free-fall time in the radiation dominated era, even if the BHs are initially on the cosmic expansion flow (Nakamura et al. 1997). The condition for forming the bound system can be written as

$$\frac{1}{\sqrt{Gm_{\rm t}}}\left(\frac{x}{1+z}\right)^{3/2} < \frac{1}{H(z)}, \tag{6}$$

where z is the cosmological redshift. Using the Friedmann equation for a flat cosmology and neglecting factors of order unity, this condition can be rewritten as

$$m_{\rm t} > \rho(z)\frac{x^3}{(1+z)^3}, \tag{7}$$

where $\rho(z)$ is the background energy density. From this expression, we can give another but equivalent physical interpretation to the criterion for forming the gravitationally bound state. The left-hand side is the total mass of the two BHs, and the right-hand side is the total mass of whatever matter component that dominates the background universe. Thus, the condition for two BHs to become gravitationally bound is equivalent to the condition for the total energy $m_{\rm t}$ to exceed the background energy contained in the comoving volume to the nearest PBH x^3.

In the radiation dominated era, the energy density of radiation can be written as

$$\rho(z) \approx \rho_{c,0}\frac{(1+z)^4}{1+z_{\rm eq}}\Omega_m, \tag{8}$$

where $z_{\rm eq}$ is the redshift at the time of matter-radiation equality, $\rho_{c,0}$ and Ω_m respectively represent a critical density and a density parameter of the non-relativistic matter at the present, and the right-hand side in Equation (7) decreases in time. Then, if x is smaller than $x_{\rm max}$ given by

$$x_{\rm max} = \left(\frac{m_{\rm t}}{\rho_{c,0}\Omega_m}\right)^{1/3}, \tag{9}$$

Equation (7) becomes satisfied at $z = z_{\rm dec} > z_{\rm eq}$, where $z_{\rm dec}$ is given by

$$1 + z_{\rm dec} = (1+z_{\rm eq})\left(\frac{x_{\rm max}}{x}\right)^3. \tag{10}$$

The physical distance of the BH pair at the time of decoupling time, which becomes the semimajor axis of the resultant binary, is given by

$$a = \frac{1}{1+z_{\rm dec}}x = Ax^4,\ A \equiv \frac{1}{1+z_{\rm eq}}\frac{1}{x_{\rm max}^3} = \frac{1}{1+z_{\rm eq}}\frac{\rho_{c,0}\Omega_m}{m_{\rm t}}. \tag{11}$$

Since the BH pair forms only for $x < x_{\rm max}$, there is an upper bound on a as $a < a_{\rm max} = x_{\rm max}/(1+z_{\rm eq})$.

If there is no force other than the gravitational force from the neighboring BHs, and the initial peculiar velocities vanish, such two BHs come closer by moving on the same straight line and end up with a head-on collision. However, in reality, there are other remote BHs surrounding the BHs in pair, and they exert a torque during the infall motion of the BHs in pair. As a result, the BH pair acquires an angular momentum, and the head-on collision is circumvented. The torque exerted by the ith distant BH to the lowest order in the distance D_i to the ith BH is given by

$$N_i = \frac{3GM_i}{2D_i^3}\sin(2\theta_i)\frac{m_1m_2}{m_{\rm t}}D^2, \tag{12}$$

where D is the physical distance between BH1 and BH2 (see Figure 1), M_i is the mass of the ith perturber BH, and θ_i is the angle between a line connecting two BHs in pair and a line connecting ith BH and a center of mass of the BH pair (see Figure 1). Thus the angular momentum generated by this torque throughout the free fall becomes

$$J_i \simeq N_i t_{\rm ff}. \tag{13}$$

Taking the direction of the torque exerted by each BH into account, the total angular momentum that the BH pair acquires is given by

$$\boldsymbol{J} = \frac{3}{2}t_{\rm ff}\frac{Gm_1m_2}{m_{\rm t}}D^2\sum_{i=1}^{N}\frac{M_i}{D_i^3}\sin(2\theta_i)\frac{(\boldsymbol{e}_z\times\boldsymbol{e}_i)}{|\boldsymbol{e}_z\times\boldsymbol{e}_i|}, \tag{14}$$

[11] In particular, we neglect the gravitational pull of the background density inhomogeneities and the forces that arise due to anisotropic accretion from the background density. We will discuss these assumptions below.

where we have chosen the line of the semi-major axis to be parallel to the z-axis and

$$\boldsymbol{e}_i = (\cos\phi_i \sin\theta_i,\ \sin\phi_i \sin\theta_i,\ \cos\theta_i) \tag{15}$$

is the unit vector pointing to the ith BH (see Figure 1). For the Keplarian motion, there is a relation between the orbital angular momentum and the eccentricity e as

$$|\boldsymbol{J}| = m_1 m_2 \sqrt{\frac{GD}{m_{\rm t}}}\sqrt{1-e^2}. \tag{16}$$

Using this formula, we obtain

$$1-e^2 = \frac{9}{4}\boldsymbol{\zeta}^2, \quad \boldsymbol{\zeta} = \sum_{i=1}^{N} \frac{x^3}{y_i^3}\frac{M_i}{m_{\rm t}} \sin(2\theta_i)\frac{(\boldsymbol{e}_z \times \boldsymbol{e}_i)}{|\boldsymbol{e}_z \times \boldsymbol{e}_i|}, \tag{17}$$

where x is the comoving distance between BH1 and BH2 and y_i is the comoving distance to the ith BH. Equations (11) and (17) are the main results of this subsection. They are the major axis and the eccentricity of the BH binary at the time of formation. Our analysis in the next subsection is based on these formulae.

Let us now estimate the value of N, namely the number of the surrounding BHs that are inside the Hubble horizon at the time of the PBH binary formation. For simplicity, only in this paragraph we assume all the PBHs have the same mass $m_{\rm BH}$ and constitute a fraction $f_{\rm PBH}$ of all the cold dark matter (for instance, $f_{\rm PBH} \simeq 10^{-3}$ is required to explain the LIGO observation; Sasaki et al. 2016). First of all, we notice that N depends on the initial comoving separation of the PBHs that form a pair. For instance, if the initial comoving separation of the BHs that form a binary is sufficiently small, they form a binary at very early time. In such a case, most likely few BHs exist inside the Hubble horizon and $N = 0$ or $N = 1$ will be the typical value. Thus, what we have to estimate is the typical value of N of PBH binaries that are relevant to observations. According to Sasaki et al. (2016), the probability dP that a given BH pair forms a binary, and then undergoes a merger at short cosmic time interval $(t, t+dt)$, is given by

$$dP = \frac{3}{16}\left(\frac{t}{T}\right)^{3/8} e(1-e^2)^{-(45/16)}\frac{dt}{t}de, \tag{18}$$

where T is defined by

$$T \equiv \frac{3}{170}\frac{{f_{\rm PBH}}^{-16/3}(Gm_{\rm BH})^{-5/3}}{(1+z_{\rm eq})^4}\left(\frac{8\pi}{3H_0^2\Omega_m}\right)^{4/3}. \tag{19}$$

For distinction between the lifetime and merger time of binaries, see the discussion around Equation (28). The merger probability for fixed t is dominated by the binaries having eccentricity near its upper limit $e_{\rm upper}$, given by Equation (11) in Sasaki et al. (2016),

$$e_{\rm upper} = \begin{cases} \sqrt{1-\left(\frac{t}{T}\right)^{\frac{6}{37}}} & \text{for } t < {f_{\rm PBH}}^{37/3}T \\ \sqrt{1-{f_{\rm PBH}}^2\left(\frac{t}{{f_{\rm PBH}}^{37/3}T}\right)^{\frac{2}{7}}} & \text{for } t \geqslant {f_{\rm PBH}}^{37/3}T. \end{cases} \tag{20}$$

We only consider the first case $t < {f_{\rm PBH}}^{37/3}T$, which is shown to be relevant to LIGO observations (Sasaki et al. 2016). For PBH mass $m_{\rm PBH} = 30\,M_\odot$, this condition becomes $f_{\rm PBH} \gtrsim 10^{-3}$. Analysis in the second case is straightforward. PBH binaries we are interested in are those that merge on the order of the age of the universe $t = t_0 \sim 1/H_0$. Then, when we fix the merger time and the eccentricity to t_0 and $e_{\rm upper}$, respectively, the semi-major axis a at the time of the binary formation is uniquely determined (see Equation (28)). Once the typical semi-major axis is determined in this way, we can convert it to the typical redshift of the PBH binary formation by using Equations (10) and (11), from which we can evaluate the number of PBHs inside the Hubble horizon at that redshift, namely N. The result is given by

$$N \sim 3\times 10^{10}\left(\frac{t}{t_0}\right)^{9/37} f_{\rm PBH}^{-26/37}\left(\frac{m_{\rm BH}}{10\,M_\odot}\right)^{-22/37}. \tag{21}$$

Thus, for the typical PBH binary with $m_{\rm PBH} = \mathcal{O}(10\,M_\odot)$ that we are interested in, there are in general more than $\sim 3\times 10^{10}$ PBHs in the Hubble horizon at the time of the binary formation if $t \simeq t_0$. Because of the weak dependence of the PBH number N on the merger time t, N is much bigger than unity for merger times relevant to observations. In what follows, we take $N \to \infty$.

One may wonder if the subsequent torque exerted on the BH binary by the surrounding BHs changes significantly the orbital parameters from the ones given by Equations (11) and (17). Considering the contribution only from the closest BH ($i = 1$) for simplicity, the angular momentum that the BH pair acquires during one period T of the orbital motion is given by

$$\Delta J = \frac{3}{2}\frac{GM_1D^2}{2D_1^3}\frac{m_1m_2}{m_{\rm t}}\sin(2\theta_1)T. \tag{22}$$

While D does not increase with the scale factor because the BH pair is gravitationally bound, the distance D_1 grows in proportion to the scale factor which scales as $\propto t^{1/2}$ in the radiation dominated epoch. Then, denoting by $D_1^{(0)}$ the initial value of D_1 at the time of binary formation, D_1 when the BH pair is in the nth cycle of the orbital motion becomes $n^{1/2}D_1^{(0)}$. The accumulated angular momentum becomes

$$J < \Delta J\sum_{n=1}^{\infty} n^{-3/2} \approx 2.6\,\Delta J. \tag{23}$$

Thus, the subsequent change of the angular momentum of the BH binary after its formation is at most a factor of $\sim$2. This factor is not important for our main result, and we do not consider this effect in the following analysis. On the other hand, note that if a distant third black hole with mass M_1 is captured on a bound orbit around the binary in a hierarchical configuration with some orbital period $T_1 \gg T$ and eccentricity e_1, it can cause significant changes in the eccentricity of the binary due to the Lidov–Kozai effect on a timescale $t_{\rm Kozai} = [(m_{\rm t}+M_1)/M_1](1-e_1^2)^{3/2}T_1^2/T$ (Naoz 2016). However, we neglect this possibility in this paper for simplicity.

There are also other effects that have been ignored in deriving Equations (11) and (17). They include peculiar velocity of the individual BH seeded in at the time of BH formation, the radiation drag, the tidal interaction with the other PBHs in the matter dominated epoch, subsequent infall of the surrounding BHs to the BH binary, tidal force from the perturbations of non-PBH dark matter, and baryon accretion onto the PBH binaries. The first three effects are investigated in Ioka et al. (1998) and were found to be subdominant. Recent

study by Ali-Haimoud et al. (2017) also confirms that the tidal forces from outer PBHs do not significantly affect the late-time evolution of PBH binaries. The subsequent infall of the surrounding BHs is also studied in Ioka et al. (1998). Ioka et al. (1998) assumed that the dark matter consists of a single-mass PBH population. In this case, the surrounding BH that caused the angular momentum of the BH binary at early times is eventually trapped by the BH binary if the outer BHs are within the mean distance of PBHs, which can be also understood from the expression of $x_{\rm max}$ given by Equation (9). Since the dynamics of the three-body problem is difficult to solve, such a case was not considered, and only the opposite case where the nearest BH is more distant than the mean distance was included in the derivation of the merger event rate in Ioka et al. (1998). Even under this restriction, it was found that the event rate is reduced at most by 40%. On the other hand, in the present case where PBHs constitute only a fraction $f_{\rm PBH}$ of all the cold dark matter, the mean distance is enhanced by a factor $f_{\rm PBH}{}^{-1/3}$ compared with the case where PBHs provide all of the dark matter. Thus the probability that the surrounding BHs are trapped by the BH binary in the latter case is smaller than the former by a factor $f_{\rm PBH}$. Because of this consideration, we make an assumption that the surrounding BHs are not gravitationally bound to the BH pair. Then, the subsequent interaction by the surrounding BH in the BH binary is not significant, and we ignore the late-time effect of the surrounding BHs in the following analysis.

The tidal force from the surrounding density perturbations of cold dark matter, not in the form of PBHs, exists when PBHs constitute only a fraction of entire dark matter. This issue was addressed by Eroshenko (2016) and Ali-Haimoud et al. (2017), who showed that the tidal effect is not significant by extrapolating the primordial perturbations on CMB scales down to the PBH scales (see also Hayasaki et al. 2016). Due to the random nature of the density perturbations, they yield additional statistically independent random contribution to $\boldsymbol{\zeta}$ in Equation (14). Since the power of the dark matter perturbation on small scales is not well understood, we do not consider this effect in this paper.

Finally, baryon accretion onto PBHs was claimed to significantly affect the PBH binaries and accelerate mergers in Hayasaki et al. (2016). But recent study by Ali-Haimoud et al. (2017), based on the simple analytic calculation, suggests that the baryon mass accumulated on PBHs in Hayasaki et al. (2016) is likely to be an overestimation and the baryonic effect is much weaker, although it may still be significant with respect to angular momentum exchange. For simplicity, we do not account for baryon accretion in this work.

3. Distribution of the Merger Rate

In the previous section, we have derived the expressions for the major axis and the eccentricity of the PBH binary in terms of the initial comoving positions and masses of PBHs. They are the basic ingredients for the evaluation of the merger rate, which is the purpose of this section.

Let us denote by $\mathcal{R}(m_1, m_2, t)$ a merger event density per unit cosmic time t and unit comoving volume in the m_1–m_2 plane. In other words,

$$\mathcal{R}(m_1, m_2, t)dm_1dm_2dtdV \tag{24}$$

represents the number of merger events of PBH binaries in the mass intervals $(m_1,\ m_1{+}dm_1)$, $(m_2,\ m_2{+}dm_2)$ that happen during $(t,\ t+dt)$ and in the comoving volume dV. Since the merger time t can be inferred from the luminosity distance (depending on the cosmological parameters), and the source frame BH masses (m_1, m_2) can be also estimated from the GW waveform, $\mathcal{R}$ is the quantity that can be in principle determined observationally. Our strategy to derive $\mathcal{R}(m_1, m_2, t)$ is described as follows. What we have to evaluate is the probability $P_{\rm intr}(m_1, m_2, t)dt$ that a given BH pair consisting of two BHs with m_1 and m_2, respectively, forms a binary, and then undergoes a merger during the short cosmic time interval $(t,\ t+dt)$. Once the quantity $P_{\rm intr}$ is obtained, using the PBH mass function given by Equation (4) and assuming that the masses of the two PBHs in the binary are independent, the merger rate density $\mathcal{R}$ is given by

$$\mathcal{R}(m_1, m_2, t) = \frac{n_{\rm BH}}{2} f(m_1) f(m_2) P_{\rm intr}(m_1, m_2, t). \tag{25}$$

The semi-major axis and the eccentricity of the BH binary at the formation time are given by Equations (11) and (17), respectively. From these equations, we see that the initial semimajor axis is a function of the random variable x as $a \equiv a(x)$ and the initial eccentricity is a function of the length of the random vector $\boldsymbol{\zeta}$ as $e \equiv e(\zeta)$, where $\zeta = |\boldsymbol{\zeta}|$. Denoting by F the probability distribution for x and ζ, the probability that the BH binary takes the values of the parameters in the range $(x,\ x+dx)$ and $(\zeta,\ \zeta+d\zeta)$ is given by

$$F(x,\ \zeta)dxd\zeta. \tag{26}$$

We can then convert this probability into the one expressed in terms of a and e as

$$F(x(a),\ \zeta(e))\frac{dx}{da}\frac{d\zeta}{de}dade. \tag{27}$$

This gives the probability that the BH binary at the formation time has the semi-major axis and the eccentricity in the range $(a,\ a+da)$, $(e,\ e+de)$.

PBH binaries shrink by emitting GWs until they finally merge. The lifetime τ of the BH binary with parameters (m_1, m_2, a, e) until it merges due to GW emission is given by (Peters 1964)[12]

$$\tau = Q(1-e^2)^{7/2}a^4, \qquad Q = \frac{3}{85}\frac{1}{G^3 m_1 m_2 m_{\rm t}}. \tag{28}$$

Denoting by $t_{\rm dec}$ the cosmic time corresponding to $z_{\rm dec}$, namely the time of binary formation, we have $\tau = t - t_{\rm dec}$. Since PBH binaries that are relevant to GW observations merge at late time $t \gg t_{\rm dec}$ ($t_{\rm dec} < 4\times10^5$ year), it is a good approximation to identify τ with t. Thus, in what follows, we replace τ in all of the expressions with t. Under this approximation, we can express a as a function of $\{\ t,\ e,\ m_1,\ m_2\}$ as $a = a(t, e, m_1, m_2)$. Using this relation, Equation (27) becomes

$$F(x(a),\ \zeta(e))\frac{dx}{da}\frac{d\zeta}{de}\frac{\partial a}{\partial t}dedt, \tag{29}$$

where it should be understood that a is replaced by $\{t, e, m_1, m_2\}$. Initial eccentricity of the BH binary is not a quantity that can be measured directly by the GW

[12] We assume that e is typically close to 1 initially, which is a good approximation in the present case.

interferometers for primordial binaries and must be integrated. There is an upper bound $e_{\rm m}$ for the initial eccentricity for fixed t because of the existence of the maximum value of the major axis $a_{\rm max} = x_{\rm max}/(1 + z_{\rm eq})$ (see Section 2.2). It is determined by the equation

$$t = Q(1 - e_{\rm m}^2)^{\frac{7}{2}} a_{\rm max}^4. \tag{30}$$

Notice that in the case of the monochromatic mass function, $e_{\rm m}$ coincides with $e_{\rm upper}$ in the second case in Equation (20). Finally, the intrinsic probability distribution is given by

$$P_{\rm intr}(m_1, m_2, t) = \int_0^{e_{\rm m}} de\, F(x(a), \zeta(e)) \frac{dx}{da}\frac{d\zeta}{de}\frac{\partial a}{\partial t}. \tag{31}$$

Having established the general framework to compute the merger rate density, let us implement this methodology in practice. It is straightforward to derive the last three factors in the integrand of Equation (31), and they are given by

$$\frac{dx}{da} = \frac{1}{4}(Aa^3)^{-1/4}, \quad \left|\frac{d\zeta}{de}\right| = \frac{2e}{3\sqrt{1-e^2}}, \tag{32}$$

$$\frac{\partial a}{\partial t} = \frac{1}{4t}\left(\frac{t}{Q}\right)^{1/4}(1 - e^2)^{-7/8}. \tag{33}$$

The highly non-trivial part is the evaluation of $F(x(a), \zeta(e))$ since $\boldsymbol{\zeta}$ depends on many random variables (in fact, an infinite number of variables) in a complicated manner. Formally, it can be written as

$$\begin{aligned} F(x(a), \zeta(e)) &= \Theta(a_{\rm max} - a)\frac{4\pi x^2(a)}{n_{\rm BH}^{-1}} \\ &\times \int \lim_{N\to\infty} \prod_{i=1}^{N} \frac{dV_i}{n_{\rm BH}^{-1}} \frac{f(M_i)dM_i}{n_{\rm BH}} \frac{\sin\theta_i d\theta_i d\phi_i}{4\pi} \\ &\times \Theta(y_i - y_{i-1}) e^{-\frac{4\pi}{3} n_{\rm BH} y_N^3} \delta(\zeta - g(x, y_i, M_i, \theta_i, \phi_i)), \end{aligned} \tag{34}$$

where $\Theta(\cdot)$ is the Heaviside step function and $\delta(\cdot)$ is the Dirac's delta function. Here, we have used the parametrization Equation (15) for $\boldsymbol{e}_i$, and introduced the notation as $y_0 = x$, $dV_i = 4\pi y_i^2 dy_i$ and

$$g(x, y_i, M_i, \theta_i, \phi_i) \equiv \left| \sum_{i=1}^{N} \frac{x^3}{y_i^3}\frac{M_i}{m_{\rm t}} \sin(2\theta_i) \frac{(\boldsymbol{e}_z \times \boldsymbol{e}_i)}{|\boldsymbol{e}_z \times \boldsymbol{e}_i|} \right|. \tag{35}$$

The derivation of Equation (34) is given in the Appendix.

We evaluate $F(x(a), \zeta(e))$ using two approximations. The first case is that only the nearest BH ($i = 1$) is incorporated in the calculation of $\boldsymbol{\zeta}$. This approximation was adopted in the previous studies (Nakamura et al. 1997; Ioka et al. 1998; Sasaki et al. 2016) for single-mass PBH mass functions. In that case, all the PBHs have the same mass, and the nearest BH ($i = 1$) exerts the strongest torque on the BH binary. Given that the torque by an outer BH is suppressed by the inverse cube of the distance, the approximation of taking only the nearest BH into account is physically natural as the zeroth order approximation.[13]

[13] The cumulative torque from all objects in a logarithmic radius bin of width $\Delta \ln y$ (e.g., here we may set $\Delta \ln y \sim \Delta y/y \sim n_{\rm BH}^{-1/3}/y$) follows from the central limit theorem and is described by a normal distribution with zero mean and root-mean-square that corresponds to $\Delta N^{1/2} g_{\rm l,rms}$, where ΔN is the number of objects in that logarithmic radius bin and $g_{\rm l,rms} = 2^{-1/2}(x/y)^{-3}(M_{\rm rms}/m_{\rm t})\sin(2\theta)_{\rm rms}$. This may be estimated roughly as $\Delta N = 4\pi n_{\rm BH} y^3 \Delta \ln y$. Therefore, the relative cumulative contribution of distant objects to the torque scales with $y^{-3/2}$, and so the smallest y dominates the integral where the number of objects is $\sim$1.

On the other hand, if the mass function is multimass, a massive outer BH may exert a stronger torque than a low-mass inner one. The wider the mass function, the more likely it is that this possibility may arise. To take into account the effect of outer perturbers, in our second estimate we consider a flat mass function up to a certain BH mass $m_{\rm max}$ and include the outer BHs to evaluate the torque.

In what follows, we evaluate $F(x(a), \zeta(e))$ and the intrinsic probability distribution for these two cases, separately.

3.1. Case 1: Torque Only from the Nearest BH

In this subsection, we make an approximation that the torque is exerted only by the nearest BH. Accordingly, the function g defined by Equation (35) becomes

$$g = \frac{x^3}{y_1^3}\frac{M_1}{m_{\rm t}} \sin(2\theta_1). \tag{36}$$

Even after this simplification, it is hard to evaluate the integral (31) analytically. For an analytic estimate, we carry out the calculation for an arbitrary but fixed value $\beta = \sin(2\theta_1)$. Our result is insensitive to the value of β, as long as it is not extremely close to zero. Since the probability of realizing $\beta \ll 1$ is suppressed (see discussion after Equation (37) for the estimation of this probability), we think that this simplification does not lose the essential feature of the merger rate density. The integral over y_1 simplifies to

$$\begin{aligned} F(x(a), \zeta(e)) &= \Theta(a_{\rm max} - a)\frac{12\pi^2 n_{\rm BH}}{1 - e^2}\beta\left(\frac{a}{A}\right)^{5/4} \\ &\times \int dM_1 f(M_1)\frac{M_1}{m_{\rm t}} \exp\left(-\frac{2\pi n_{\rm BH} M_1}{\sqrt{1-e^2}\, m_{\rm t}}\left(\frac{a}{A}\right)^{3/4}\beta\right) \\ &\times \Theta\left(\frac{M_1}{m_{\rm t}}\beta - \frac{2}{3}\sqrt{1-e^2}\right). \end{aligned} \tag{37}$$

The PBH binaries at the time of their formation are highly eccentric ($e \approx 1$). Since the PBH mass function is implicitly assumed to be narrow in the present case, M_1 does not differ from $m_{\rm t}$ significantly, and the argument of the last Heaviside function is positive unless β is smaller than $\frac{2}{3}\frac{m_{\rm t}}{M_1}\sqrt{1-e^2}$. Now, let us estimate the probability that β becomes smaller than the critical value β_c for which the argument of the Heaviside function becomes zero. To this end, we again consider the monochromatic mass function and use the eccentricity given by the first case of Equation (20). Then, β_c becomes

$$\beta_c \simeq 0.01 \times f_{\rm PBH}^{16/37}\left(\frac{t}{t_0}\right)^{3/37}\left(\frac{m_{\rm BH}}{10\,M_\odot}\right)^{5/37}. \tag{38}$$

For $\beta_c \ll 1$, the probability that β happens to be smaller than β_c is approximately given by

$$P(\beta < \beta_c) \approx \frac{\beta_c^2}{16} \simeq 6 \times 10^{-6}, \tag{39}$$

for the fiducial values used in Equation (38). This probability is much smaller than unity, and we replace the last Heaviside function by 1 in the following analysis. Then, the intrinsic

probability distribution (31) becomes

$$P_{\rm intr}(m_1, m_2, t) = \frac{1}{8t}\int dM_1 \frac{1}{\beta}\frac{m_{\rm t}}{M_1}K^2\frac{f(M_1)}{n_{\rm BH}} \times \int_0^{e_{\rm m}} de\, e(1-e^2)^{-\frac{45}{16}} \times \exp\left[-K(1-e^2)^{-\frac{37}{32}}\right], \quad (40)$$

where we have introduced a dimensionless parameter K by

$$K \equiv 2\pi n_{\rm BH}\frac{M_1}{m_{\rm t}}A^{-\frac{3}{4}}\left(\frac{t}{Q}\right)^{\frac{3}{16}}\beta. \quad (41)$$

This is a small parameter. For instance, for a single-mass PBH mass function with mass $m_{\rm BH}$ and the Hubble time $t = 1/H_0$, we have

$$K = \left(\frac{170}{3}\right)^{\frac{3}{16}}\left(\frac{3}{\pi}\right)^{\frac{1}{4}}(1+z_{\rm eq})^{\frac{3}{4}}\pi\Omega_m^{\frac{1}{4}}f_{\rm PBH}(Gm_{\rm BH}H_0)^{\frac{5}{16}}\beta \sim 3\times 10^{-4} f_{\rm PBH}\beta\left(\frac{m_{\rm BH}}{10M_\odot}\right)^{\frac{5}{16}}, \quad (42)$$

where $f_{\rm PBH}$ is the mass fraction of the PBHs to the entire cold dark matter

The integration over e can be expressed in terms of the incomplete gamma function. Then, Equation (40) becomes

$$P_{\rm intr}(m_1, m_2, t) = \frac{2}{37t}\int dM_1 \frac{1}{\beta}\frac{m_{\rm t}}{M_1}\frac{f(M_1)}{n_{\rm BH}}K^{\frac{16}{37}} \times \left[G(K) - G\left(\frac{M_1}{m_c}\right)\right], \quad (43)$$

where m_c and $G(x)$ are defined by

$$m_c \equiv \frac{m_{\rm t}}{2\pi n_{\rm BH}}\frac{1}{\beta}\left(\frac{t}{Q}\right)^{1/7}(1+z_{\rm eq})^{4/7}\left(\frac{\rho_{c,0}\Omega_m}{m_{\rm t}}\right)^{\frac{25}{21}}, \quad (44)$$

$$G(x) = \Gamma\left(\frac{58}{37}, x\right). \quad (45)$$

For the monochromatic mass function, m_c is given by

$$m_c \sim 7\times 10^{-4}M_\odot\,(f_{\rm PBH}\beta)^{-1}\left(\frac{m_{\rm BH}}{10M_\odot}\right)^{\frac{26}{21}}. \quad (46)$$

Equation (43) for arbitrary $f(M)$ mass function is the final expression of the intrinsic merger probability distribution in the present case.

3.2. Case 2: Torque from the Outer BHs

Let us next consider the case in which the PBH mass function is flat from $m_{\rm min} = \epsilon m_{\rm max}$ to $m_{\rm max}$ and vanishes outside of it. As mentioned earlier, we implicitly assume that $\epsilon \gtrsim 0.1$. Then the PBH mass function is given by

$$f(m) = \frac{1}{m_{\rm max}(1-\epsilon)}\Theta(m_{\rm max}-m)\Theta(m-m_{\rm min}). \quad (47)$$

We include not only the nearest BH but also outer BHs.

It is extremely difficult to perform the integration of Equation (34) analytically.[14] However, we can estimate the approximate behavior of $F(x, \zeta)$ in the domain $n_{\rm BH}x^3 \ll 1$, where the PBH binaries with lifetime comparable to the age of the universe form.[15] To this end, let us first write $F(x, \zeta)$ as

$$F(x,\zeta) = \frac{4\pi x^2}{n_{\rm BH}^{-1}}e^{-\frac{4\pi}{3}n_{\rm BH}x^3}P(x,\zeta), \quad (48)$$

where $P(x, \zeta_0)d\zeta$ is a probability that ζ takes value in the interval $(\zeta_0, \zeta_0+d\zeta)$ for given x. For later convenience, let us define $\tilde{\zeta}$ by $(m_{\rm t}/m_{\rm max})\,\zeta$. Thus, we have

$$F(x,\zeta) \approx 4\pi n_{\rm BH}x^2\tilde{P}(x,\tilde{\zeta})\frac{m_{\rm t}}{m_{\rm max}}, \quad (49)$$

where $\tilde{P}(x, \tilde{\zeta}_0)d\tilde{\zeta}$ is the probability that $\tilde{\zeta}$ takes a value in the interval $(\tilde{\zeta}_0, \tilde{\zeta}_0 + d\tilde{\zeta})$ for given x. Looking at the definition of $\boldsymbol{\zeta}$, we expect that the typical value of $\tilde{\zeta}$ for given x is around $n_{\rm BH}x^3$, since y_i $(i = \mathcal{O}(1))$ is typically about $n_{\rm BH}^{-1/3}$ and the contribution from y_i with higher i is suppressed (see footnote 13). Noting that $y_i > x$, the case in which $\zeta \ll n_{\rm BH}x^3$ is realized by either if $y_1 \gg n_{\rm BH}^{-1/3}$ or if accidental cancellation takes place among terms with different i. Since the former is suppressed exponentially as $\sim e^{-\frac{4\pi}{3}n_{\rm BH}y_1^3}$, the latter, which is stochastic, dominates. Recalling that $\boldsymbol{\zeta}$ is essentially a two-dimensional vector, the probability that $\tilde{\zeta}$ is in the thin ring $(\tilde{\zeta}, \tilde{\zeta} + d\tilde{\zeta})$ by the random choice is proportional to the ring area, namely $\tilde{\zeta}d\tilde{\zeta}$. Thus, we expect

$$\tilde{P}(x,\tilde{\zeta}) \propto \tilde{\zeta}, \quad (50)$$

for $\tilde{\zeta} \ll n_{\rm BH}x^3$. On the other hand, the case $\tilde{\zeta} \gg n_{\rm BH}x^3$ is realized mainly when y_1 is accidentally much smaller than the typical value $n_{\rm BH}^{-1/3}$. The probability of such a situation is controlled by the volume element $y_1^2dy_1$, and the relation $\tilde{\zeta} \propto y_1^{-3}$ leads to $y_1^2dy_1 \propto \tilde{\zeta}^{-2}d\tilde{\zeta}$. Thus, we expect

$$\tilde{P}(x,\tilde{\zeta}) \propto \tilde{\zeta}^{-2}, \quad (51)$$

for $\tilde{\zeta} \gg n_{\rm BH}x^3$. From the definition of $\boldsymbol{\zeta}$ given by Equation (17), we have

$$\sigma^2 \equiv \langle\boldsymbol{\zeta}^2\rangle = \frac{32\pi}{135}\left(\frac{m_{\rm max}}{m_{\rm t}}\right)^2 n_{\rm BH}x^3(1+\epsilon+\epsilon^2). \quad (52)$$

The derivation of this result is given in Appendix. One simple function that interpolates Equations (50) and (51) is given by

$$\tilde{P}(x,\tilde{\zeta}) = \frac{3\sqrt{3}}{2\pi}\xi^{1/3}\tilde{\sigma}^2\frac{\tilde{\zeta}}{\tilde{\zeta}^3+\xi\tilde{\sigma}^6}, \quad (53)$$

where $\tilde{\sigma} = (m_{\rm t}/m_{\rm max})\sigma$, $\xi = \mathcal{O}(1)$ is a fitting parameter, and the normalization condition is imposed.

In order to check the validity of the approximation (53), we evaluate $\tilde{P}(x, \tilde{\zeta})$ numerically by the Monte Carlo method. For this purpose, we first fix N and x. Then, we randomly generate a set of random variables $\{M_i, y_i, \theta_i, \phi_i\}$ and compute $\tilde{\zeta}$. By

[14] Analytic expression of the probability distribution for the eccentricity was derived for the monochromatic mass function in Ali-Haimoud et al. (2017).

[15] PBH binaries with $n_{\rm BH}x^3 \sim 1$ have a larger semimajor axis and more circular orbit than those with $n_{\rm BH}x^3 \ll 1$. These two factors make the lifetime of the binaries much longer than the age of the universe.

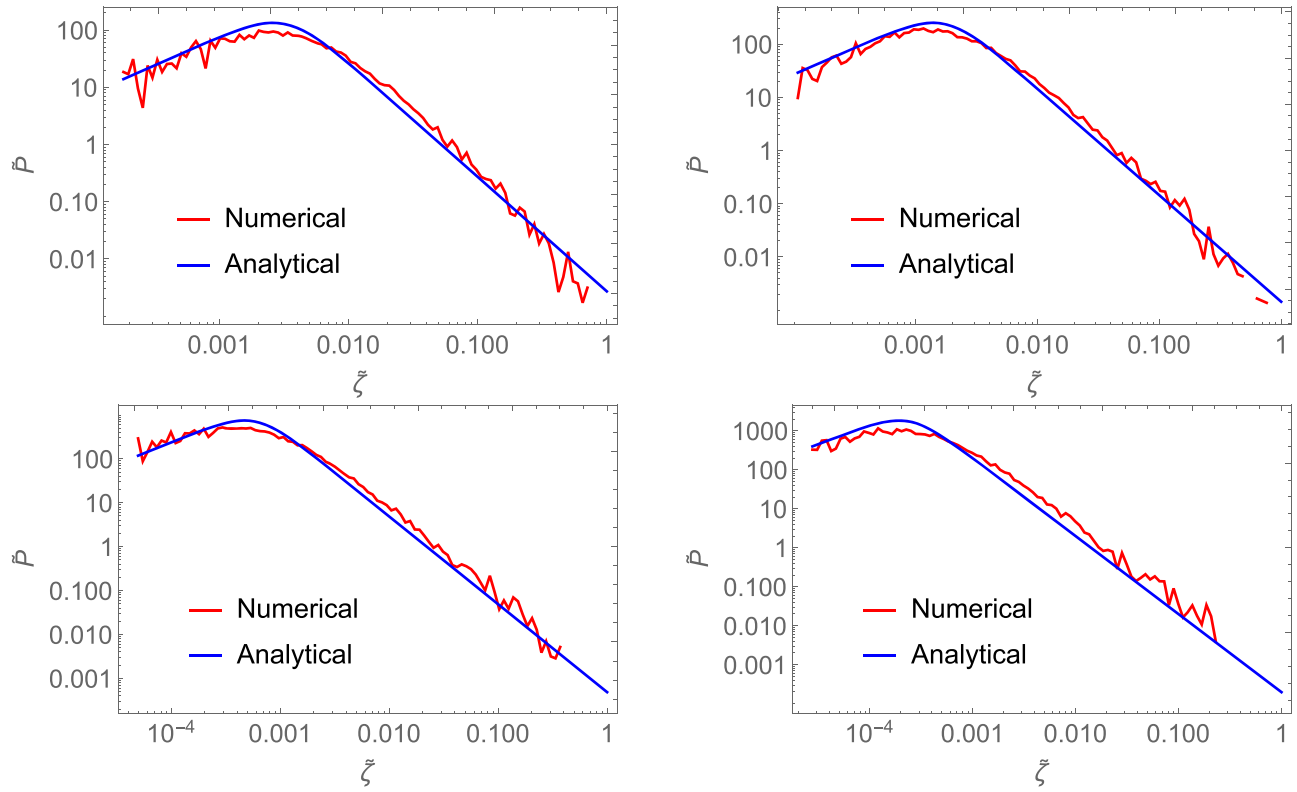

Figure 2. Red curves represent the probability distribution $\tilde{P}(x, \tilde{\zeta})$ of 10,000 Monte Carlo realizations of the dimensionless torque parameter $\tilde{\zeta}$ for four different values of $\frac{4}{3}\pi n_{\rm BH} x^3 = 10^{-2}$ (top-left panel), 5×10^{-3} (top-right panel), 2×10^{-3} (bottom-left panel), and 10^{-3} (bottom-right panel) with $N = 5$ perturbing BHs for a flat PBH mass function (47) with $\epsilon = 0.1$. Here $n_{\rm BH}$ and x is the comoving PBH number density and initial comoving distance between BHs that form binary, respectively. Blue curves represent the probability distribution given by Equation (53) with $\xi = 5.5$.

repeating this process many times, we obtain the distribution of $\tilde{\zeta}$ for a given N and x up to the statistical uncertainty.

Figure 2 shows the distribution of 10,000 realizations of $\tilde{\zeta}$ for $N = 5$ for $\epsilon = 0.1$, $\frac{4\pi}{3} n_{\rm BH} x^3 = (10^{-2}, 5 \times 10^{-3}, 2 \times 10^{-3}, 10^{-3})$. The red curve represents the distribution obtained by the Monte Carlo calculations, and blue one represents the analytic approximation (53) with $\xi = 5.5$. We find that this simple ansatz of $\tilde{P}(x, \tilde{\zeta})$ fairly recovers the numerically obtained probability distribution. Although we consider the flat mass function, we expect that the ansatz should work qualitatively for other mass functions since the asymptotic behaviors (50) and (51) are determined independently of the mass function. In what follows, we adopt Equation (53). Then, $F(x, \zeta)$ becomes

$$F(x, \zeta) = 6\sqrt{3}\,\xi^{1/3} n_{\rm BH} \tilde{\sigma}^2 \zeta x^2 \left(\frac{m_{\rm t}}{m_{\rm max}}\right)^2 \times \left[\left(\frac{m_{\rm t}}{m_{\rm max}}\right)^3 \zeta^3 + \xi \tilde{\sigma}^6\right]^{-1}. \quad (54)$$

Substituting $F(x, \zeta)$ given by Equation (54) into Equation (31), after some algebra, we obtain

$$P_{\rm intr} = \frac{135\sqrt{3}}{256\pi t} \frac{1}{\xi^{1/3}(1 + \epsilon + \epsilon^2)} \nu^{\frac{16}{37}} \frac{m_{\rm t}}{m_{\rm max}} \int_{w_{\rm m}}^{\infty} \frac{w^{\frac{21}{32}}}{w^{\frac{111}{32}} + 1} dw. \quad (55)$$

Here we have defined a dimensionless quantity ν by

$$\nu = \frac{16\pi}{45} \xi^{1/3} (1 + \epsilon + \epsilon^2) n_{\rm BH} \frac{m_{\rm max}}{m_{\rm t}} A^{-3/4} \left(\frac{t}{Q}\right)^{\frac{3}{16}}, \quad (56)$$

and we have changed the integration variable as $w = \nu^{-32/37}(1 - e^2)$, and $w_{\rm m} = \nu^{-32/37}(1 - e_{\rm m}^2)$. Using a relation $n_{\rm BH} = 2\rho_{\rm BH}/(m_{\rm max}(1 + \epsilon))$, which is valid for a flat mass function, we have

$$w_{\rm m} = \left(\frac{32\pi}{45} \gamma^{1/3} \frac{1 + \epsilon + \epsilon^2}{1 + \epsilon}\right)^{-\frac{32}{37}} (1 + z_{\rm eq})^{\frac{128}{259}} f_{\rm PBH}^{-\frac{32}{37}} \times \left(\frac{\rho_{c,0}\Omega_m}{m_{\rm t}}\right)^{\frac{128}{777}} \left(\frac{G^3 m_1 m_2 m_{\rm t}}{3} t\right)^{\frac{32}{259}}. \quad (57)$$

To estimate typical magnitude of $w_{\rm m}$, for equal mass binary ($m_1 = m_2 = m_{\rm BH}$), $w_{\rm m}$ is given by

$$w_{\rm m} \approx 2 \times 10^{-4} f_{\rm PBH}^{-\frac{32}{37}} \left(\frac{m_{\rm BH}}{M_\odot}\right)^{\frac{160}{777}}. \quad (58)$$

This shows that $w_{\rm m}$ can be bigger or smaller than unity within the range of the feasible values of $f_{\rm PBH}$ and $m_{\rm BH}$. Although the integration over w in Equation (55) can be expressed in terms of the hypergeometric function, we do not write it explicitly here since it gives no useful information. Thus, Equation (55) is the final expression of the intrinsic merger rate and the main result of this subsection.

4. Hidden Universality in the Merger Rate Density

In the previous section, we have derived the analytic expression of $P_{\rm intr}$ in the m_1–m_2 plane for the two different limiting cases corresponding to the different approximations. According to Equation (25), the observable merger rate density is not $P_{\rm intr}$, but $P_{\rm intr}$ weighted by the PBH mass function. The observable merger event density is highly dependent on the PBH mass function, and it appears at first glance that no definite prediction can be extracted for the PBH scenario without choosing the specific mass function. Contrary to this naive guess, there is a unique feature expressed as a mathematical relation for the differentiated merger rate density specific to the PBH scenario, as we will show below. Such a relation could be quite useful as a powerful method for testing the PBH scenario when the sufficient number of merger events have been accumulated.

Let us first consider the case where $P_{\rm intr}$ is given by Equation (40). This expression of $P_{\rm intr}$ still contains the integration over the PBH mass nearest to the BH binary. Although this integration cannot be done explicitly without choosing the specific PBH mass function, carrying out the explicit integration is not needed for our present purpose. The function $G(x)$ appearing in the integrand is monotonically decreasing, and its asymptotic behavior is given as

$$G(x)=\begin{cases}\frac{21}{37}\Gamma\left(\frac{21}{37}\right)-\frac{37}{58}x^{\frac{58}{37}}+\mathcal{O}(x^{\frac{95}{37}}), & (x\ll 1)\\ x^{\frac{21}{37}}e^{-x}(1+\mathcal{O}(x^{-1})). & (x\gg 1).\end{cases} \tag{59}$$

Using this formula and noting that K, which is much smaller than unity according to Equation (42), is always less than M_1/m_c, we find that the integrand of Equation (40) becomes

$$\begin{aligned}&\frac{m_{\rm t}}{M_1}\frac{f(M_1)}{n_{\rm BH}}K^{\frac{16}{37}}\left[G(K)-G\left(\frac{M_1}{m_c}\right)\right]\\ &=\begin{cases}\frac{37}{58}\frac{m_{\rm t}}{M_1}\frac{f(M_1)}{n_{\rm BH}}K^{\frac{16}{37}}\left(\frac{M_1}{m_c}\right)^{\frac{58}{37}}, & \frac{M_1}{m_c}<1\\ \frac{21}{37}\Gamma\left(\frac{21}{37}\right)\frac{m_{\rm t}}{M_1}\frac{f(M_1)}{n_{\rm BH}}K^{\frac{16}{37}}, & \frac{M_1}{m_c}>1.\end{cases}\end{aligned} \tag{60}$$

A crucial consequence of these approximate expression is that the integrand has a simple scaling property with m_1 and m_2. Using the scalings,

$$K\propto {m_{\rm t}}^{-\frac{1}{16}}(m_1m_2)^{\frac{3}{16}},\qquad m_c\propto {m_{\rm t}}^{-\frac{1}{21}}(m_1m_2)^{\frac{1}{7}}, \tag{61}$$

we find that the above integrand scales as

$$\begin{aligned}&\frac{m_{\rm t}}{M_1}\frac{f(M_1)}{n_{\rm BH}}K^{\frac{16}{37}}\left[G(K)-G\left(\frac{M_1}{m_c}\right)\right]\\ &\propto\begin{cases}{m_{\rm t}}^{\frac{22}{21}}(m_1m_2)^{-\frac{1}{7}}, & \frac{M_1}{m_c}<1\\ {m_{\rm t}}^{\frac{36}{37}}(m_1m_2)^{\frac{3}{37}}, & \frac{M_1}{m_c}>1.\end{cases}\end{aligned} \tag{62}$$

Because of this factorization, the same scaling for m_1m_2 and $m_{\rm t}$ remains for $P_{\rm intr}$. Assuming one of the branches ($M_1<m_c$ or $M_1>m_c$) dominates the integral, $P_{\rm intr}$ scales as

$$P_{\rm intr}(m_1,m_2,t)\propto\begin{cases}{m_{\rm t}}^{\frac{22}{21}}(m_1m_2)^{-\frac{1}{7}}, & (M_1<m_c\ \text{dominates})\\ {m_{\rm t}}^{\frac{36}{37}}(m_1m_2)^{\frac{3}{37}}, & (M_1>m_c\ \text{dominates}).\end{cases} \tag{63}$$

Then, the observable merger rate density $\mathcal{R}$ per unit time and unit volume defined by Equation (25) can be written as

$$\begin{aligned}&\mathcal{R}(m_1,m_2,t)\\ &=\begin{cases}C_A{m_{\rm t}}^{\frac{22}{21}}h_A(m_1)h_A(m_2), & (M_1<m_c\ \text{dominates})\\ C_B{m_{\rm t}}^{\frac{36}{37}}h_B(m_1)h_B(m_2), & (M_1>m_c\ \text{dominates}),\end{cases}\end{aligned} \tag{64}$$

where $h_A(m)\equiv m^{-\frac{1}{7}}f(m)$, $h_B(m)\equiv m^{\frac{3}{37}}f(m)$ and C_A, C_B are quantities that are independent of m_1 and m_2, but contain information of $f(m)$. An interesting point of Equation (64) is that the dependence of the merger rate density on the total mass $m_{\rm t}$ is independent of the model-dependent functions $h_A(m)$ or $h_B(m)$ (namely, mass function) and is completely determined as $\propto {m_{\rm t}}^{36/37}$ for the former case and $\propto {m_{\rm t}}^{22/21}$ for the latter case. The mass function enters the game only through the total normalization constant (represented as C_A and C_B) and the factorizable part $h_A(m_1)$ $h_A(m_2)$ or $h_B(m_1)$ $h_B(m_2)$. Thus, by focusing on the total mass part of merger rate density and picking it up, we can provide a definite prediction for the merger rate density that is insensitive to the shape and amplitude of the PBH mass function. Indeed, we can pick up the total mass part by taking the logarithm of $\mathcal{R}$ and then differentiating it by m_1 and m_2, namely,

$$\begin{aligned}\alpha(m_1,m_2,t)&\equiv -{m_{\rm t}}^2\frac{\partial^2}{\partial m_1\partial m_2}\ln\mathcal{R}(m_1,m_2,t)\\ &=\begin{cases}\frac{36}{37}, & (M_1<m_c\ \text{dominates})\\ \frac{22}{21}, & (M_1>m_c\ \text{dominates})\end{cases}\end{aligned} \tag{65}$$

for any (m_1, m_2). As discussed at the beginning of Section 3, the merger rate density $\mathcal{R}$ can be determined in principle by observations if a sufficient number of BH merger events are detected and the potential detection bias can be appropriately eliminated. Thus, the quantity α on the left-hand side can be also determined observationally. In this sense, the left-hand side can be determined by observations. Our PBH merger scenario predicts that this quantity is equal to $36/37$ for the upper case and $22/21$ for the lower case. In reality, what is realized lies between the above two cases, and the left-hand side of Equation (65) may take a value between the two values corresponding to the upper case and the lower case, respectively. Given that the numerical values on the right-hand side for both cases are close to 1 (within less than 5%), the left-hand side of Equation (65) in the mixture case would be also close to 1. Taking into account this possibility, we conclude that under the assumption of the uniform spatial distribution of PBHs the merger rate density satisfies the

following relation:

$$\frac{36}{37} \leqslant \alpha(m_1, m_2, t) \leqslant \frac{22}{21}. \quad (66)$$

This relation is robust in the sense that it is independent of the underlying mass function.

A similar conclusion can be drawn to the second case where $P_{\rm intr}$ is given by Equation (55). In this case, the observable merger rate density (Equation (25)) is given by

$$\mathcal{R} = \frac{135\sqrt{3}}{512\pi t} \frac{\nu^{\frac{16}{37}}}{\xi^{1/3}(1+\epsilon+\epsilon^2)(1-\epsilon)^2} \times \frac{n_{\rm BH}}{m_{\rm max}^2} \frac{m_{\rm t}}{m_{\rm max}} \int_{w_{\rm m}}^{\infty} \frac{w^{\frac{21}{32}}}{w^{\frac{111}{32}}+1} dw. \quad (67)$$

As we have done in the case 1, let us evaluate the integral for two limiting cases ($w_{\rm m} \ll 1$ and $w_{\rm m} \gg 1$), separately.

First, when $w_{\rm m} \ll 1$, we can extend the lower limit of the integral to 0. As a result, we obtain

$$\mathcal{R} = \frac{C_1}{t} \nu^{\frac{16}{37}} \left(\frac{n_{\rm BH}}{m_{\rm max}}\right)^2 \frac{m_{\rm t}}{m_{\rm max}}, \quad (68)$$

where C_1 is a constant of order unity. Using the scaling for ν as (see Equation (56))

$$\nu \propto m_{\rm t}^{-\frac{1}{16}} (m_1 m_2)^{\frac{3}{16}}, \quad (69)$$

$\mathcal{R}$ can be written as

$$\mathcal{R}(m_1, m_2, t) = \tilde{C}_1 m_{\rm t}^{\frac{36}{37}} h_1(m_1) h_1(m_2), \quad (70)$$

where $h_1(m) \equiv m^{\frac{3}{37}} f(m)$ and $\tilde{C}_1$ is a quantity that is independent of m_1, m_2, but contains information of $f(m)$. As with the above discussion for the case 1, $\mathcal{R}$ has a unique dependence on $m_{\rm t}$. This dependence can be again extracted by considering the quantity α as

$$\alpha(m_1, m_2, t) = \frac{36}{37}. \quad (71)$$

This value precisely coincides with the lower end of Equation (66).

Let us next investigate the case $w_{\rm m} \gg 1$. In this case, we obtain

$$\mathcal{R} \approx \frac{C_2}{t} \nu^{\frac{16}{37}} \left(\frac{n_{\rm BH}}{m_{\rm max}}\right)^2 \frac{m_{\rm t}}{m_{\rm max}} w_{\rm m}^{-\frac{29}{16}}, \quad (72)$$

where C_2 is a constant of order unity. Using the scaling for $w_{\rm m}$ as (see Equation (57))

$$w_{\rm m} \propto m_{\rm t}^{-\frac{32}{777}} (m_1 m_2)^{\frac{32}{259}}, \quad (73)$$

as well as that for ν, we find

$$\mathcal{R}(m_1, m_2, t) = \tilde{C}_2 m_{\rm t}^{\frac{22}{21}} h_2(m_1) h_2(m_2), \quad (74)$$

where $h_2(m) \equiv m^{-\frac{1}{7}} f(m)$ and $\tilde{C}_2$ is a quantity that is independent of m_1, m_2, but contains information of $f(m)$. Then, we find

$$\alpha(m_1, m_2, t) = \frac{22}{21}. \quad (75)$$

This value precisely coincides with the upper end of Equation (66). Thus, the range of α in the present case is also given by Equation (66).

To summarize, our study demonstrates that $0.97 \lesssim \alpha \lesssim 1.05$ holds in the considered PBH scenario in which PBHs form binaries in the early universe. The uncertainty in α is small enough to distinguish the PBH scenario from different scenarios for explaining the origin of the merging BH binaries once a sufficiently large number of merger events are measured. For instance, Bird et al. (2016) considered the formation of PBH binaries due to close encounters in dark matter halos at low redshifts. This PBH scenario gives a different merger rate density, that is (Raidal et al. 2017),

$$\mathcal{R}(m_1, m_2, t) = C m_1^{\frac{2}{7}} f(m_1)\, m_2^{\frac{2}{7}} f(m_2)\, m_{\rm t}^{\frac{10}{7}}, \quad (76)$$

where C is a quantity independent of m_1 and m_2. For this process, Equation (2) gives

$$\alpha = \frac{10}{7} \approx 1.43. \quad (77)$$

Thus, this scenario predicts a unique and different value from the one studied in this paper. Gondán et al. (2017b) has recently extended this analysis to systems in collisional equilibrium where mass segregation takes places such as in galactic nuclei. In this case, α is a unique function of the total binary mass. Another example is the astrophysical scenario in which the BH binaries form and evolve due to dynamical encounters in dense stellar environments. In this scenario, O'Leary et al. (2016) found that approximately $P_{\rm intr} = \mathcal{R}(m_1, m_2)/[f(m_1)f(m_2)] \propto m_{\rm t}^4$. In this case, the higher mass mergers are much more probable mainly due to the mass dependence of binary formation during chance triple encounters, exchange interactions, mass segregation, and dynamical hardening effects. If the intrinsic merger probability does not depend on the symmetric mass ratio $\eta = m_1 m_2/(m_1+m_2)^2$, then we get $\alpha = 4$ for this process. Clearly, a $\alpha \sim 4$ value is largely outside of the region obtained for both PBH scenarios mentioned above. When a sufficient number of mergers accumulates to determine α, it may be possible to exclude several formation scenarios and pin down the most likely scenario.

In order to crudely estimate the necessary sample size to measure α from future GW detections, we generate a mock Monte Carlo sample of BHs drawn from a fiducial flat mass function between a range of masses 5 and 30 $M_\odot$, and generate a random merger sample by randomly drawing objects with probability proportional to $(m_1+m_2)^\alpha$. For this order-of-magnitude estimate, we neglect the measurement error of mass, since the mass measurement accuracy is expected to be much smaller than the range of BH masses (i.e., $\Delta m_{1,2}/m_{1,2} \sim 25\%$) for half of the sources for the design sensitivity of second generation GW instruments, including Advanced LIGO, Advanced VIRGO, and KAGRA (Ghosh et al. 2016).[16] We generate a 2D histogram of events and fit the value of α. Repeating this analysis 1000 times for fixed fiducial α gives an approximate posterior distribution function of the measured α. This analysis shows that a

[16] If heavy BHs exist with mass $30\,M_\odot < m_{1,2} < 50\,M_\odot$, the median mass measurement errors are expected to be of order 40% (Vitale et al. 2017).

sample of 100 events is necessary to measure α to integer accuracy, and 1000 events would allow us to measure it with an error of 0.15 if the fiducial value of α is between 1 and 3. The current rate estimates predict $\mathcal{R} = 12$–$240\,\mathrm{Gpc^{-3}\,yr^{-1}}$. Assuming a maximum detection distance of $z = 0.5$ for the design sensitivity of second generation instruments, a sample of $\sim$100 events (1000 events) will accumulate in between 6 and 120 days (60 days and 3.3 years).

5. Summary

There is a growing interest in the possibility that the merging BHs detected by LIGO are primordial. Previous studies (Sasaki et al. 2016) showed that the BH binary merger event rate estimated by LIGO can be explained by the PBHs, which constitute only a tiny fraction of the entire dark matter. While the estimated masses of the individual BHs show some spread $10 \sim 30\,M_\odot$, it was assumed in the previous study that all the PBHs have the same mass of $30\,M_\odot$. Although this is a reasonable approximation when only the first event for which masses of two BHs in the binary are almost the same is observationally known, it hugely compresses the valuable information about the event rate distribution in the BH mass plane.

In this paper, we extended the formalism to compute the merger event rate to the case where the PBH mass function is not monochromatic. Our basic assumption on the mass function made throughout this paper is that it is not widely extended over many orders of magnitude in the BH mass range but is confined to the mass range $\sim 10\,M_\odot$. The derived formula (31) contains multiple integrations over many random variables (Equation (34)) and is complicated enough to defeat the exact analytic computation. Based on the physical expectation that among remote BHs the closest one gives the largest torque on average, we evaluated the simplified version of Equation (31) in which only the closest BH is taken into account. In this case, the computation becomes much more feasible. We found that the quantity α constructed from the merger rate density $\mathcal{R}$ in the BH mass plane as

$$\alpha(m_1, m_2, t) \equiv -(m_1 + m_2)^2 \frac{\partial^2}{\partial m_1 \partial m_2} \ln \mathcal{R}(m_1, m_2, t) \quad (78)$$

becomes almost independent of the PBH mass function and takes a value close to unity ($0.97 \lesssim \alpha \lesssim 1.05$). Since it is possible that several distant BHs generate the dominant torque instead of the closest one during binary formation in the early universe, we have also considered the case in which the remote BHs are taken into account for a flat PBH mass function. Even in this case, we found that the quantity α exactly coincides with the one derived for the case of the closest perturbing BH. This suggests that the determined value of α is robust to observationally test the PBH scenario once a large sample of mergers becomes available with accurately determined masses.

Other astrophysical mechanisms leading to BH mergers are generally expected to yield different α values. Recently, O'Leary et al. (2016) has shown that the probability of merger is proportional to m_t^4 for binary BH mergers in dense star clusters, which implies $\alpha \sim 4$ if the merger rates are nearly independent to mass ratio. PBH binaries formed in the low redshift universe by GW emission during close encounters lead to $\alpha \approx 1.43$ (Bird et al. 2016). BH binaries formed by GW emission in mass-segregated environments such as galactic nuclei lead to α values that vary with the total binary mass m_t (Gondán et al. 2017b).

The mass distribution is not the only GW observable that allows one to distinguish between different mechanisms leading to binary BH mergers. For instance, it was shown recently that PBHs are unlikely to possess large spins (Chiba & Yokoyama 2017). When the statistics of BH spins are accumulated in the future, this will also become a powerful discriminator. Further, the eccentricity distribution will be useful to distinguish binaries formed by GW capture in high velocity dispersion environments at low redshifts (O'Leary et al. 2009; Gondán et al. 2017a). The observable PBH binaries that formed at high redshifts are expected to have close to zero eccentricity due to circularization by GW emission (Peters 1964). *LISA* will be able to determine the eccentricity for mergers with $e \gtrsim 10^{-6}$ (Seto 2016). Detection of BHs with masses less than $\sim 1\,M_\odot$, which may be possible with the advanced LIGO, VIRGO, and KAGRA at design sensitivity, would provide strong evidence of the existence of PBHs (Clesse & García-Bellido 2017b; Magee & Hanna 2017). Finally, future GW detectors will allow us to map out the cosmological luminosity distance (or redshift) distribution for BH mergers to high redshifts (Nakamura et al. 2016; Koushiappas & Loeb 2017b). Examining the multidimensional GW event rate distribution will be essential to prove or disprove the PBH scenario.

This work was supported by MEXT KAKENHI Nos. 17H06357 (TT and TS), 17H06358 (TT), 17H06359 (TS), 15H05888 (TS and SY), 15H02087 (TT), and 15K21733 (TS and SY), JSPS Grant-in-Aid for Young Scientists (B) No.15K17632 (TS) and No.15K17659 (SY), and the Grant-in-Aid for Scientific Research No. 26287044 (TT). This project has received funding from the European Research Council (ERC) under the European Union's Horizon 2020 research and innovation programme under grant agreement No. 638435 (GalNUC), and by the Hungarian National Research, Development, and Innovation Office grant NKFIH KH-125675 (BK). This work was performed in part at the Aspen Center for Physics, which is supported by National Science Foundation grant PHY-1607761.

Appendix
Derivation of the Probability Distribution

The non-trivial part of Equation (34) is the probability distribution for x and $y_i\,(i = 1, \cdots, N)$, and we focus on this part only.

Let $P(N, V)$ be the probability that there are N BHs in the volume V. For BHs that are uniform randomly distributed, we have

$$P(N, V) = \frac{1}{N!}\left(\frac{V}{V_0}\right)^N e^{-V/V_0}, \quad (79)$$

where V_0 is the volume for which the expectation particle number is 1. Thus,

$$V_0 = n_{\mathrm{BH}}^{-1}. \quad (80)$$

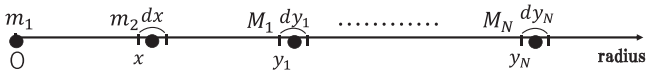

Figure 3. This figure describes a situation where the individual BHs with mass m_1, m_2, M_1, $\cdots$ and M_N locate at the origin, $(x, x+dx)$, (y_1, y_1+dy_1), $\cdots$, and (y_N, y_N+dy_N), respectively.

Then, the probability that the situation shown in Figure 3 is realized is given by

$$\begin{aligned} dP &= P\left(0, \frac{4\pi}{3}x^3\right)\frac{d\left(\frac{4\pi}{3}x^3\right)}{V_0}P\left(0, \frac{4\pi}{3}y_1^3 - \frac{4\pi}{3}x^3\right) \\ &\quad\times \frac{d\left(\frac{4\pi}{3}y_1^3\right)}{V_0}\cdots P\left(0, \frac{4\pi}{3}y_N^3 - \frac{4\pi}{3}y_{N-1}^3\right)\frac{d\left(\frac{4\pi}{3}y_N^3\right)}{V_0} \\ &= \frac{4\pi x^2 dx}{V_0}\frac{4\pi y_1^2 dy_1}{V_0}\cdots\frac{4\pi y_N^2 dy_N}{V_0}\exp\left(-\frac{4\pi y_N^3}{3V_0}\right). \end{aligned} \tag{81}$$

From the definition of ζ in Equation (17), we have

$$\begin{aligned} \langle\zeta^2\rangle &= \frac{x^6}{m_t^2}\sum_{i=1}^{N}\sum_{j=1}^{N}\left\langle\frac{1}{y_i^3}\frac{1}{y_j^3}\right\rangle\langle M_i M_j\rangle \\ &\quad\times\left\langle\sin(2\theta_i)\sin(2\theta_j)\frac{(\boldsymbol{e}_z\times\boldsymbol{e}_i)}{|\boldsymbol{e}_z\times\boldsymbol{e}_i|}\cdot\frac{(\boldsymbol{e}_z\times\boldsymbol{e}_j)}{|\boldsymbol{e}_z\times\boldsymbol{e}_j|}\right\rangle. \end{aligned} \tag{82}$$

Using Equation (15) for $\boldsymbol{e}_i$, we obtain

$$\left\langle\sin(2\theta_i)\sin(2\theta_j)\frac{(\boldsymbol{e}_z\times\boldsymbol{e}_i)}{|\boldsymbol{e}_z\times\boldsymbol{e}_i|}\cdot\frac{(\boldsymbol{e}_z\times\boldsymbol{e}_j)}{|\boldsymbol{e}_z\times\boldsymbol{e}_j|}\right\rangle = \frac{8}{15}\delta_{ij}. \tag{83}$$

By the assumption that M_i obeys the uniform distribution in the interval $(\epsilon\, m_{\max}, m_{\max})$, we have

$$\langle M_i^2\rangle = \frac{1}{3}m_{\max}^2(1+\epsilon+\epsilon^2). \tag{84}$$

Thus, we obtain

$$\langle\zeta^2\rangle = \frac{8}{45}\frac{x^6}{m_t^2}m_{\max}^2(1+\epsilon+\epsilon^2)\sum_{i=1}\left\langle\frac{1}{y_i^6}\right\rangle. \tag{85}$$

The calculation of $\sum_{i=1}\langle 1/y_i^6\rangle$ can be done by noting that it is an expectation value of $1/y^6$ where y is the distance of particles randomly distributed in the region $y > x$ (Ioka et al. 1998),

$$\lim_{N\to\infty}\sum_{i=1}^{N}\left\langle\frac{1}{y_i^6}\right\rangle = \int_x^\infty\frac{4\pi y^2 dy}{n_{\rm BH}^{-1}}\frac{1}{y^6} = \frac{4\pi}{3}\frac{n_{\rm BH}}{x^3}. \tag{86}$$

Plugging this result into Equation (85) finally yields

$$\langle\zeta^2\rangle = \frac{32\pi}{135}n_{\rm BH}x^3\left(\frac{m_{\max}}{m_t}\right)^2(1+\epsilon+\epsilon^2). \tag{87}$$

References

Abbott, B. P., Abbott, R., Abbott, T. D., et al. 2016a, ApJL, 818, L22
Abbott, B. P., Abbott, R., Abbott, T. D., et al. 2016b, PhRvX, 6, 041015
Abbott, B. P., Abbott, R., Abbott, T. D., et al. 2016c, PhRvL, 116, 061102
Abbott, B. P., Abbott, R., Abbott, T. D., et al. 2016d, ApJL, 833, L1
Abbott, B. P., Abbott, R., Abbott, T. D., et al. 2017a, PhRvL, 118, 221101
Abbott, B. P., Abbott, R., Abbott, T. D., et al. 2017b, ApJL, 851, L35
Abbott, B. P., Abbott, R., Abbott, T. D., et al. 2017c, PhRvL, 119, 141101
Ali-Haimoud, Y., & Kamionkowski, M. 2017, PhRvD, 95, 043534
Ali-Haimoud, Y., Kovetz, E. D., & Kamionkowski, M. 2017, PhRvD, 96, 123523
Bird, S., Cholis, I., Muñoz, J. B., et al. 2016, PhRvL, 116, 201301
Brandt, T. D. 2016, ApJL, 824, L31
Byrnes, C. T., Copeland, E. J., & Green, A. M. 2012, PhRvD, 86, 043512
Carr, B., Kuhnel, F., & Sandstad, M. 2016, PhRvD, 94, 083504
Carr, B., Raidal, M., Tenkanen, T., Vaskonen, V., & Veermäe, H. 2017, PhRvD, 96, 023514
Carr, B. J. 1975, ApJ, 201, 1
Carr, B. J. 2005, in 59th Yamada Conf. Inflating Horizon of Particle Astrophysics and Cosmology, ed. H. Suzuki et al. (Tokyo: Universal Academy Press, Inc.), 129
Carr, B. J., & Hawking, S. W. 1974, MNRAS, 168, 399
Chiba, T., & Yokoyama, S. 2017, PTEP, 2017, 083E01
Choptuik, M. W. 1993, PhRvL, 70, 9
Clesse, S., & García-Bellido, J. 2017a, PDU, 15, 142
Clesse, S., & García-Bellido, J. 2017b, arXiv:1711.10458
Custodio, P. S., & Horvath, J. E. 1998, PhRvD, 58, 023504
Eroshenko, Yu. N. 2016, arXiv:1604.04932
Fishbach, M., & Holz, D. E. 2017, ApJL, 851, L25
Gaggero, D., Bertone, G., Calore, F., et al. 2017, PhRvL, 118, 241101
Ghosh, A., Del Pozzo, W., & Ajith, P. 2016, PhRvD, 94, 104070
Gondán, L., Kocsis, B., Raffai, P., & Frei, Z. 2017a, arXiv:1705.10781
Gondán, L., Kocsis, B., Raffai, P., & Frei, Z. 2017b, arXiv:1711.09989
Green, A. M. 2017, PhRvD, 96, 043020
Harada, T., Yoo, C.-M., & Kohri, K. 2013, PhRvD, 88, 084051
[Erratum: 2014, PhRvD, 89, 029903]
Hayasaki, K., Takahashi, K., Sendouda, Y., & Nagataki, S. 2016, PASJ, 68, 66
Horowitz, B. 2016, arXiv:1612.07264
Inoue, Y., & Kusenko, A. 2017, JCAP, 1710, 034
Ioka, K., Chiba, T., Tanaka, T., & Nakamura, T. 1998, PhRvD, 58, 063003
Kashlinsky, A. 2016, ApJL, 823, L25
Koushiappas, S. M., & Loeb, A. 2017a, PhRvL, 119, 041102
Koushiappas, S. M., & Loeb, A. 2017b, PhRvL, 119, 221104
Kovetz, E. D., Cholis, I., Breysse, P. C., & Kamionkowski, M. 2017, PhRvD, 95, 103010
Magee, R., & Hanna, C. 2017, ApJL, 845, L13
Mandel, I., Farr, W. M., Colonna, A., et al. 2017, MNRAS, 465, 3254
Matsumoto, T., Teraki, Y., & Ioka, K. 2017, arXiv:1704.05047
Miller, M. C. 2016, GReGr, 48, 95
Nakamura, T., Ando, M., Kinugawa, T., et al. 2016, PTEP, 2016, 093E01
Nakamura, T., Sasaki, M., Tanaka, T., & Thorne, K. S. 1997, ApJL, 487, L139
Naoz, S. 2016, ARA&A, 54, 441
Niemeyer, J. C., & Jedamzik, K. 1998, PhRvL, 80, 5481
O'Leary, R. M., Kocsis, B., & Loeb, A. 2009, MNRAS, 395, 2127
O'Leary, R. M., Meiron, Y., & Kocsis, B. 2016, ApJL, 824, L12
Peters, P. C. 1964, PhRv, 136, B1224
Poulin, V., Serpico, P. D., Calore, F., Clesse, S., & Kohri, K. 2017, PhRvD, 96, 083524
Raidal, M., Vaskonen, V., & Veermäe, H. 2017, JCAP, 1709, 037
Sasaki, M., Suyama, T., Tanaka, T., & Yokoyama, S. 2016, PhRvL, 117, 061101
Seto, N. 2016, MNRAS, 460, L1
Vitale, S., Lynch, R., Raymond, V., et al. 2017, PhRvD, 95, 064053
Yokoyama, J. 1998, PhRvD, 58, 107502
Young, S., & Byrnes, C. T. 2013, JCAP, 1308, 052
Zevin, M., Pankow, C., Rodriguez, C. L., et al. 2017, ApJ, 846, 82